This is a repository copy of *Enhancing the solvent resistance and thermomechanical properties of thermoplastic acrylic polymers and composites via reactive hybridisation*.

Enhancing the solvent resistance and thermomechanical properties of thermoplastic acrylic polymers and composites via reactive hybridisation

Winifred Obande [a], Weronika Gruszka [b], Jennifer A. Garden [b], Christian Wurzer [c], Conchúr M. Ó Brádaigh [a], Dipa Ray [a,*]

[a] School of Engineering, Institute for Materials and Processes, The University of Edinburgh, Sanderson Building, Robert Stevenson Road, Edinburgh EH9 3FB, Scotland, United Kingdom
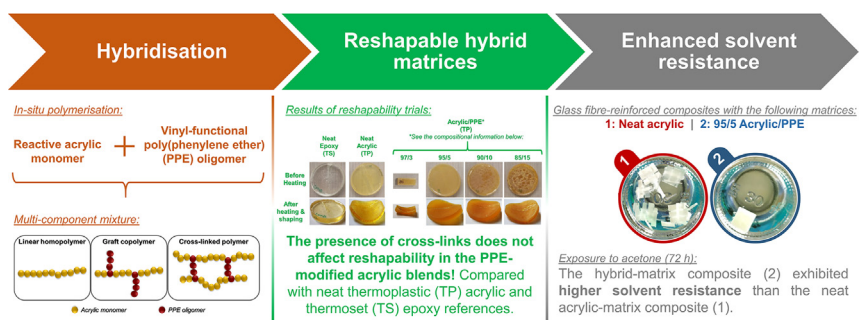[b] EaStCHEM School of Chemistry, The University of Edinburgh, Joseph Black Building, David Brewster Road, Edinburgh EH9 3FJ, Scotland, United Kingdom
[c] School of GeoSciences, UK Biochar Research Centre, The University of Edinburgh, Edinburgh EH9 3FF, Scotland, United Kingdom

HIGHLIGHTS

- Reactive acrylic/poly(phenylene ether) (PPE) blends were studied.
- Acrylic-PPE blends exhibited improved solvent resistance.
- Room-temperature vacuum processing of glass fibre-acrylic/PPE was demonstrated.
- Acrylic/PPE blends maintained full reshapability upon heating after polymerisation.

GRAPHICAL ABSTRACT

ABSTRACT

This work demonstrates the use of an engineering thermoplastic, poly(phenylene ether) (PPE) to enhance the solvent resistance and thermomechanical properties of liquid acrylic resin-based composites by a reactive hybridisation route. Oligomeric PPE with vinyl functionality was employed to attain chemical reactivity between the two constituents during the in-situ polymerisation process. Both unreinforced polymer blends and glass fibre-reinforced composites were studied; physical insights into the polymer structure and properties were obtained through complementary spectroscopic analysis, thermal analysis and microscopy. Spectroscopic analysis revealed the formation of multi-component mixtures in the blends, containing both $CDCl_3$-soluble and -insoluble constituents, with the latter likely corresponding to a reacted acrylic/PPE species. These findings show that incorporating reactive PPE into a reactive acrylic resin to produce a hybrid-matrix system is a simple, yet effective strategy towards enhancing solvent resistance (mass retention: 98% – PPE-modified; 72% – unmodified), while simultaneously enhancing the glass transition temperature (+9%) in acrylic-matrix composites.

© 2021 Published by Elsevier Ltd. This is an open access article under the CC BY-NC-ND license (http://creativecommons.org/licenses/by-nc-nd/4.0/).

1. Introduction

Processing methodologies for thermoplastic polymer matrix composites can be expensive for low part volumes, owing to high melt-viscosity, which must be overcome with high-cost tooling at elevated temperatures and pressures. More recently, a family

of monomeric acrylic resins, which are suited to liquid resin infusion (LRI) processing of composites at room temperature, has become the subject of extensive research [1–9]. Such research efforts have focused on benchmarking their mechanical and thermomechanical performance against those of commodity-to-intermediate-performance epoxy systems. It has been established that the acrylic composites exhibit comparable performance with their epoxy counterparts [1,10–22].

Acrylics, as amorphous commodity thermoplastic polymers, are highly susceptible to solvent attack [23], which makes them unsuitable for application in particular environments. Improved solvent resistance can be highly beneficial for acrylic matrix composites, increasing their acceptance in a broader range of applications. This is particularly of importance in automotive applications, where solvent and chemical resistance are desirable in composite matrices to overcome the effects of prolonged in-service exposure to chemicals such as gasoline, motor oil, antifreeze, paint, cleaning solvents and road salts [24]. Moreover, in terms of their thermomechanical performance, lower glass transition temperatures have been reported (compared to epoxy-based composites) [19]. Thus, any efforts to enhance solvent resistance should ideally maintain or increase the glass transition temperature and overall thermal stability.

Low-viscosity, liquid thermoplastic acrylic resins are ideal candidate materials for the reactive modification methodologies employed for liquid thermosetting resin systems in composite applications [25–33]. Notably, liquid thermosetting resins can be used as reactive solvents within which higher molecular weight (higher performance) thermoplastics can be dissolved for subsequent processing by liquid composite moulding methods. This is an attractive way to produce composite structures from hybrid matrices with tailored performance [34,35].

The novelty of this current work compared with previous publications lies in the following aspects. *First*, the attainment of solvent-resistant blends using a telechelic PPE oligomer with chain-end vinyl functionality to promote reactivity with a liquid thermoplastic acrylic resin. *Second*, the ability to obtain said blends without compatibilisers or intermediates [36,37], and without sacrificing thermal stability and thermomechanical performance. *Third*, the direct application of oligomeric PPE as a co-reactant with a reactive, liquid acrylic monomer to produce room-temperature vacuum-infused composite laminates. Ultimately, the findings presented herein open up opportunities for new applications of acrylic/PPE-matrix composites, such as their potential use for components requiring in-service or periodic exposure to harsh chemical and thermal conditions. Examples include body and structural parts in automobiles, where the risk of contact with fuels, lubricants and cleaners/disinfectants may be significant enough to limit the drop-in replacement of thermosetting resin systems with thermoplastic acrylic resins.

To this end, the present work combines complementary analytical techniques to assess the effects of hybridisation on the chemical structure, phase morphology, solvent resistance and thermal characteristics of the PPE-modified acrylic materials, compared to an unmodified acrylic polymer counterpart. Solvent resistance and thermomechanical properties are evaluated in both unreinforced and reinforced forms.

2. Materials and methods

2.1. Materials

A liquid thermoplastic acrylic resin (Elium® 188O – Arkema GRL, France) was reactively modified with an oligomeric PPE to investigate an innovative route for modifying these liquid resins for composite applications. The PPE used was NORYL™ SA9000 resin (SABIC) – a low-molecular-weight grade (number average molecular weight (M_n): 2300 Da) with vinyl functional groups. Hereafter, the polymer samples (unmodified reference and blends) will be referred to as A100/P0, A97/P3, A95/P5, A90/P10, A85/P15 and A0/P100 as per the compositions and identification scheme: A#/P*, where # and * are weight fractions of acrylic and PPE in the blend, respectively.

The composite laminates described in Section 2.2.2 are reinforced by a glass, non-crimp fabric (TEST2594) supplied by Ahlstrom-Munksjö Glassfibre OY, Finland, where GF is appended to the designation defined for the unreinforced polymers and polymer blends to imply the use of glass fibre reinforcement. The glass fabric had a quasi-unidirectional construction, comprising 1200 TEX 0°-fibres (94%), 68 TEX 90°-fibres (6%) and polyester stitching. A [0]$_8$ preform was assembled using eight plies, laid up symmetrically about the mid-plane of the laminate. For both unreinforced polymers and reinforced composites, polymerisation was initiated with a dibenzoyl peroxide initiator (BP50FT) supplied by United Initiators GmbH, Germany.

2.2. Sample preparation

2.2.1. Unreinforced polymer and polymer blends

PPE was dissolved into liquid acrylic resin in the compositional range of 3% to 15% by weight of the acrylic resin. The liquid acrylic resin acted as a reactive solvent for the PPE oligomer. BP50FT, a dibenzoyl peroxide (BPO) initiator was added to the resin blends 24 h after preparation at a mix ratio of 100:3 (by weight). The same initiator content was used for the neat acrylic resin. Samples measuring 50 mm × 8 mm × 4 mm (nominally) were polymerised at room temperature for 24 h in silicone moulds. Polytetrafluoroethylene (PTFE)-covered steel plates were used to cover the moulds throughout the polymerisation to prevent the evaporation and foaming of the liquid resin. The sample specifications used for characterisation are provided in the relevant methodology sections of this paper.

2.2.2. Glass fibre-reinforced composites

To assess the potential enhancements conferred by using the PPE-modified acrylic matrix for composite applications, glass fibre-reinforced acrylic and PPE-modified acrylic laminates were also produced by vacuum infusion processing as detailed in the supporting information (Section S1). The PPE-modified acrylic laminate composition was selected based on the miscibility and phase stability trial results in the supplementary material (Section S1, Figure S1), which revealed 5 wt% (A95/P5) as the most stable blend for the resin infusion conditions employed in this work. Hereafter, the laminates will be referred to as GF/A100/P0 and GF/A95/P5. The burn-off technique was employed to determine their fibre volume fractions as 49.5% and 57%, and fibre weight fractions of 68% and 75%, respectively. The corresponding void contents for these materials were 0.4% and 0.8%, respectively. Their solvent resistance and thermomechanical behaviour have been comparatively assessed and will be discussed in Sections 3.1.2 and 3.2.2, respectively. Average thicknesses for the GF/A100/P0 and GF/A95/P5 were 3.8 mm and 3.3 mm, respectively. For solvent resistance studies, samples measuring 8 mm × 8 mm were used, whereas, for thermomechanical analysis, nominal sample dimensions were 40 mm × 8 mm.

2.3. Solvent resistance characterisation by prolonged acetone immersion

Non-standard solvent resistance experiments were performed in acetone to study the influence of PPE-modifier content on the

unreinforced acrylic matrix system. Two independent sets of experiments were conducted (one sample per material type, per set); polymerised samples of unmodified acrylic and acrylic/PPE blends (PPE content: 3–15 wt%) were sectioned, weighed (216–275 mg) and placed in acetone at room temperature for 60 min and 72 h. Samples with a 60-min exposure time were immersed in acetone for the test duration and carefully removed, dried and weighed after completing the experiment. Data collection for the 72-h study involved routine inspections at set intervals up to 300 min, during which visible geometrical changes were recorded until the end of the experiment. After 300 min had elapsed, samples were inspected at the 24-h mark and 72-h mark. All coupons were removed from the solvent, dried and weighed at the end of the respective test durations. The same procedure was followed for glass fibre-reinforced composite samples (GF/A100/P0 and GF/A95/P5) with starting weights of 410 – 490 mg to assess their comparative resistance to acetone.

2.4. Characterisation of thermomechanical properties by dynamic mechanical analysis

The dynamic mechanical analysis (DMA) was performed on polymer samples to study the influence of PPE-modifier content on T_g and damping behaviour using a DMA 8000 analyser (Perkin Elmer, USA). Two samples (per set), measuring 40 mm $\times$ 8 mm $\times$ 4 mm (nominal dimensions) were dynamically loaded at a fixed frequency of 1 Hz using a dual cantilever bending configuration. Each sample was heated from ambient temperature to 180°C at 3°C/min.

2.5. Thermogravimetric analysis of unreinforced polymer and polymer blend samples

Thermogravimetric analysis (TGA) was performed using a TGA/DSC 1 analyser (Mettler Toledo, USA) to analyse the thermal stability of polymeric samples. Samples weighing 10 mg were heated from 25°C to 600°C at 10°C/min under a nitrogen flow rate of 50 ml/min. The evolution of mass loss and derivative thermograms (DTG) were compared. Results are averages of duplicates (two samples per material).

2.6. Confocal Raman microscopy of fractured polymer blend surfaces

Fractured samples were non-destructively imaged using a Confocal Raman microscopy technique to spatially assess the chemical composition of each blend. This method was complementary to the rest of the characterisation methods, as it provided insights into the phase morphology and interactions between the blend components. Single polymeric samples were fractured using the non-standard flexural testing method described by Obande et al. [38]. To enhance the visualisation precision across the fracture surface (irrespective of topographical variations), the sample was maintained at constant focus using a *TrueSurface*® tool. An Alpha 300 AR instrument (WiTec GmbH, Germany) was used for this study.

2.7. Solution-state nuclear magnetic resonance (NMR) spectroscopy of polymer and polymer blend samples

The chemical structures of unmodified acrylic and PPE in the presence and absence of BPO (i.e., polymers and unpolymerised liquid resins, respectively), as well as acrylic/PPE blends (PPE content: 5–10 wt%), were analysed using ^{1}H and 2D NMR experiments (^{1}H–^{1}H COrrelated SpectroscopY (COSY), ^{1}H–^{13}C Heteronuclear Single Quantum Coherence (HSQC) spectroscopy and Diffusion-Ordered SpectroscopY (DOSY)). NMR spectra were recorded on a Bruker AVA500 (USA) spectrometer at 298 K (500 MHz) in CDCl$_3$ and were referenced to the residual CDCl$_3$ peaks (^{1}H: δ 7.26 ppm, ^{13}C: 77.2 ppm). Only the soluble portions of the reactive A95/P5 and A90/P10 blends were analysed by NMR spectroscopy in CDCl$_3$. The solubility of the reactive blends in CDCl$_3$ was improved by heating (50°C) and sonicating the blends in CDCl$_3$ for approximately 2 h or leaving the samples in excess CDCl$_3$ overnight. Both blends also exhibited low solubility in other common NMR spectroscopy solvents (tetrahydrofuran (THF)-d_8, pyridine d_5 and toluene d_8).

3. Results and discussions

3.1. Solvent resistance

### 3.1.1. Unreinforced polymer and polymer blend samples

Fig. 1 shows the results of solvent resistance experiments on unreinforced polymers. Following exposure to acetone for 60 min at room temperature, all acrylic/PPE blend polymer samples exhibited lower mass losses after 60 min in acetone than the unmodified acrylic (A100/P0) sample. A 37% mass loss was observed with the A100/P0 sample, whereas the blends sustained mass losses in the range of 10–18 %. Except for the A97/P3 sample, which lost only 12% of its original mass, an increase in PPE content from 5 wt% (A95/P5) to 15 wt% (A85/P15) results in a consistent increase in solvent resistance, evidenced by corresponding terminal mass losses of 18% and 10%, respectively.

Following the 72-h exposure experiments, the A100/P0 was found to completely dissolve after 300 min, following a visible, progressive loss of volume. In contrast, all blends sustained only 23–25% of mass loss, showing significant improvements in their solvent resistance. Increasing PPE concentration within the blends did not, however, appear to result in significant changes in the terminal mass in acetone after 72 h. These observations provide strong evidence that PPE content plays a vital role in the dissolution rate and consequently, initial mass loss of acrylic/PPE blends.

The dissolution rate of polymers is influenced by polymer characteristics such as molecular weight, the chemical structure and composition of the polymer backbone, segmental stiffness, and dispersity. Given that the addition of PPE into the hybrid matrices adds aromatic groups within their structure, where the unmodified acrylic only contains aliphatic polymer chains, obvious differences in backbone structure, composition, molecular weight and segmental stiffness are likely to arise between the polymer matrices. The variations in initial dissolution behaviour observed in the 60-min experiments with increasing PPE content are possibly linked with differences in polymer chain mobility [39,40]. At a molecular level, the variation of respective chain mobilities may be substantial enough to give rise to varying reptation times and thus, disengagement rates. This may provide evidence of interchain interactions between the phenyl groups within the PPE modifier.

Moreover, the A100/P0 sample can be seen to undergo progressive mass loss until complete dissolution at 300 min. In contrast, the PPE-modified hybrid matrices appear to exhibit whitening, with considerable swelling being observed across all samples until the full study duration elapsed. These results suggest a significant effect of PPE incorporation on the molecular weight [40] and the possibility of cross-linked [41] acrylic/PPE species arising from the reactions of monomeric acrylic with multi-vinyl oligomeric PPE. Moreover, dispersity also plays a role in the rate of dissolution and may explain the enhanced solvent resistance observed with the hybrid matrices [40].

It is worth noting that white sediments were observed in the solvent from 60 min for all hybrid matrices. These sediments remained in solution until the experiment was completed. The size of dispersed sediment appeared to increase with increasing PPE
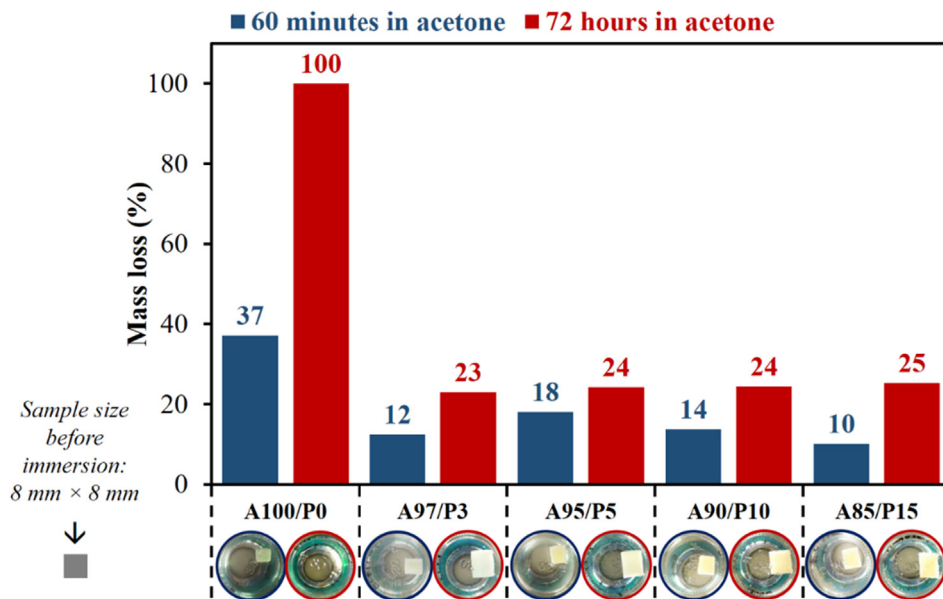
Fig. 1. Results of solvent resistance experiments after exposure of unreinforced polymer samples to acetone for 60 min (blue) and 72 h (red). Mass losses are presented for unmodified acrylic (A100/P0) and PPE-modified acrylic (A97/P3-A85/P15) where a lower mass loss corresponds to superior solvent resistance. Note: results are based on one sample per material, per set. (For interpretation of the references to colour in this figure legend, the reader is referred to the web version of this article.)

content. These observations may indicate the presence of unreacted oligomeric PPE within the polymerised samples, which is in agreement with observations from NMR analysis of these materials, as discussed in Section 3.5.
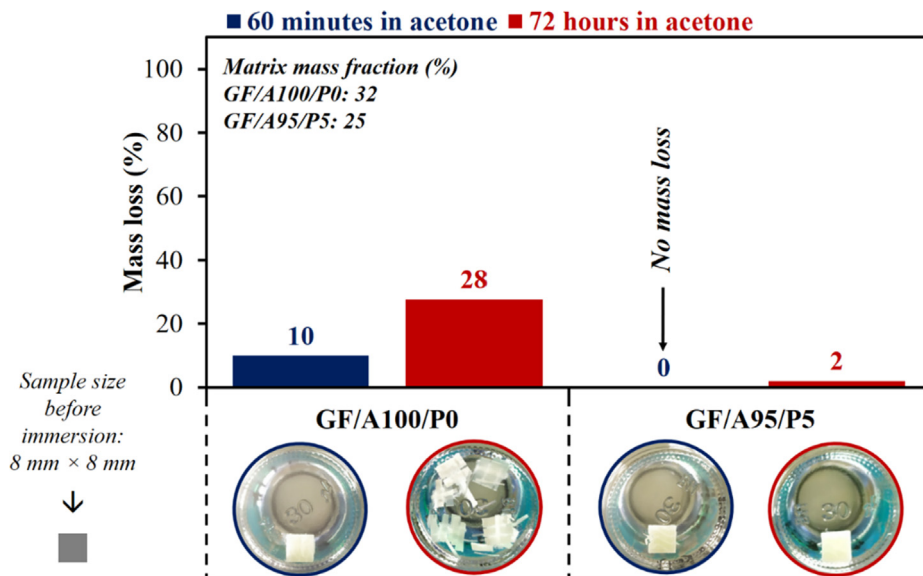
3.1.2. Glass-fibre reinforced composite samples

Fig. 2 shows the results of solvent resistance experiments on glass fibre-reinforced acrylic (GF/A100/P0) and acrylic/PPE (GF/A95/P5) composite samples. 60-min solvent resistance experiments on the fibre-reinforced acrylic (GF/A100/P0) and acrylic/PPE (GF/A95/P5) revealed that the incorporation of PPE into the acrylic resin system contributes positively to the resistance to initial solvent ingress and subsequent dissolution. No evidence of

mass loss was measured after 60 min. In the unmodified acrylic composite sample (GF/A100/P0), a 10% loss in mass was recorded.

Given that the rate of dissolution is influenced by chain mobility at a molecular scale, these results suggest significant differences in the reptation times and disengagement rates [39,40] between both matrices. The differences in respective chain mobilities may be substantial enough to give rise to varying reptation times and disengagement rates at a molecular level. These variations can result from the presence of the cross-linked species or the presence of phenyl moieties within the backbone.

Following the longer time-scale exposure (72 h), it becomes clear that the use of the PPE-modified matrix results in even more significant improvement of the solvent resistance of the GF/A95/P5

Fig. 2. Mass losses after the exposure of glass fibre-reinforced acrylic (GF/A100/P0) and PPE-modified acrylic (GF/A95/P5) composite samples to acetone for 60 min (blue) and 72 h (red) showing the influence of PPE modifier content on solvent resistance. Note: A lower mass loss corresponds to superior solvent resistance. (For interpretation of the references to colour in this figure legend, the reader is referred to the web version of this article.)

(only 2% of mass loss) over its unmodified acrylic counterpart (GF/A100/P0), which lost 28% of its original mass. With a matrix mass fraction of 32 ± 0.3% in the composite, this recorded mass loss for the GF/A100/P0 sample is similar in magnitude to its matrix mass fraction. As such, it indicates that complete dissolution of the acrylic matrix occurred, which is in agreement with visual observations during data collection (Fig. 2).

3.2. Characterisation of thermomechanical properties by dynamic mechanical analysis

3.2.1. Unreinforced polymer and polymer blend samples

From single-frequency DMA scans at 1 Hz, the effects of PPE-modification on the glass transition temperatures and tan delta peak heights were studied alongside the unmodified acrylic polymer matrix material. T_g values were determined as the temperatures corresponding to the maximum tan delta values. The representative thermograms obtained from each material presented in Fig. 3a reveal single tan delta peaks for all blends. A lowering effect was also observed for the tan delta peak heights, with values decreasing by up to ~ 0.2 (-12%). These trends are more pronounced up to 5 wt% addition of PPE, as in the A95/P5 material; however, as PPE content is increased up to 15 wt% (A85/P15), the contributions are less prominent. Moreover, a mild T_g shift is evident with increasing PPE content. Given that the PPE used had a higher T_g (160°C) than the acrylic constituent, such a shift is expected with the in-situ polymerisation of acrylic in the presence of PPE.

Increasing the PPE content within the blends causes an overall increase in T_g by up to ~ 6°C (Fig. 3c). This suggests decreased chain mobility owing to increased rigidity and π- π interactions due to

the phenyl rings [42] of the PPE phase. Given that tan delta is a ratio of loss modulus to storage modulus, and describes the degree of viscoelastic damping within a material and the extent of polymer segmental mobility, the overall reductions in tan delta peak height with increasing PPE content suggests a reduction in the viscoelastic response of the blends compared to the unmodified acrylic polymer matrix.

The reductions in tan delta peak height may be due to increased rigidity caused by the phenyl moieties in PPE or may indicate the existence of a cross-linked species, which would likely decrease the chain mobility [43]. Despite the absence of a cross-linking agent, the presence of vinyl-functionalised PPE oligomer may have triggered spontaneous localised cross-linking alongside the formation of a non-cross-linked acrylic-rich constituent. Using a high-molecular-weight vinyl-pendant PPO, Huang et al. [44] proposed that a higher vinyl-pendant ratio was more likely to undergo a cross-linking reaction during polymerisation than a lower ratio. Interestingly, increasing glass transition temperatures were also thought to be attributed to the presence of cross-links within the vinyl-pendant PPO structure.

While this present research employed a low-molecular-weight, vinyl-end-functionalised PPE, it is plausible that increased glass transition temperatures in the blends with respect to A100/P0 was a contribution of cross-linked structures.

The effects of PPE modification on half peak width and peak factor were also assessed. Half peak width is typically used to evaluate the relative reduction of relaxation-induced molecular mobility [45]. Peak factor is a representation of the intrinsic heterogeneity within the polymer system [46]. It is calculated as the ratio of the corresponding half peak width (Fig. 3b) and peak height (Fig. 3b) for each material. Within blended polymeric systems with
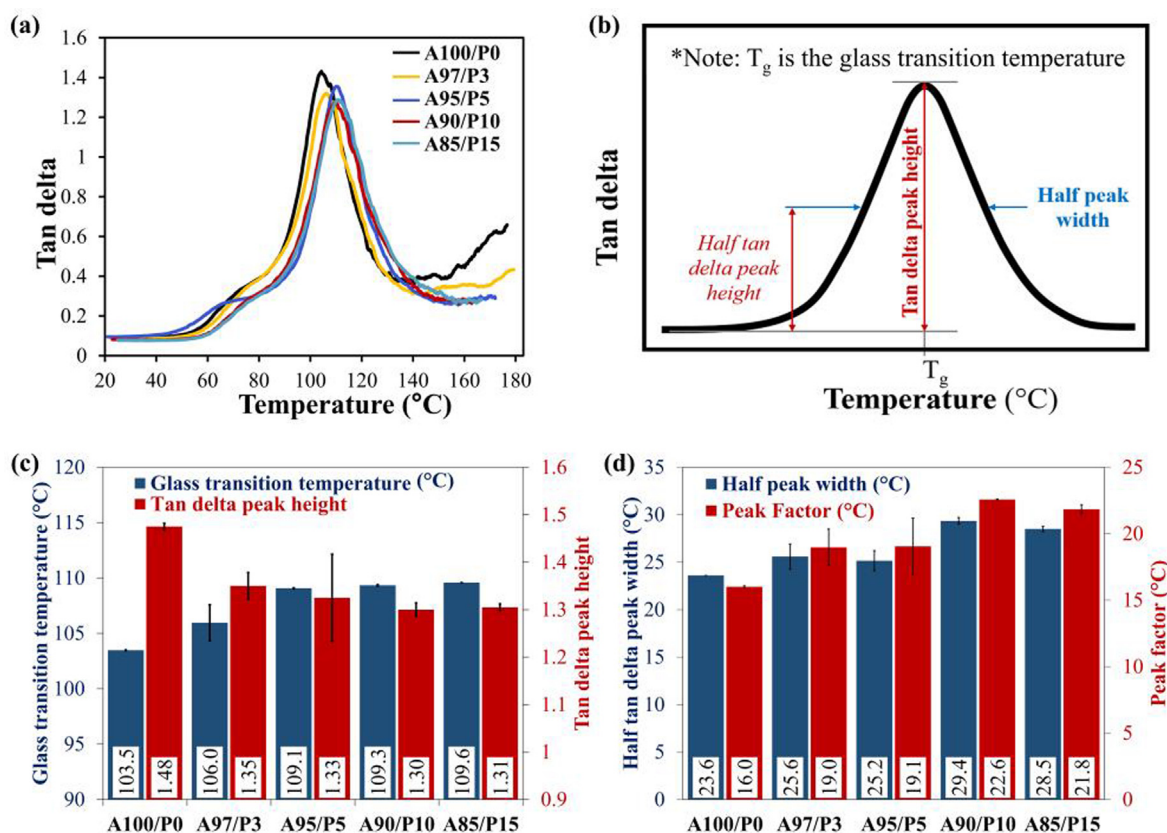

Fig. 3. (a) Representative DMA results, showing the effects of PPE content on damping behaviour (tan delta) and T_g, (b) graphical representation of the reported parameters, (c) T_g values and tan delta peak heights, and (d) half tan delta peak widths and peak factors from DMA experiments on polymer matrix samples. Results are averages of duplicates.

dissimilar T_g values, broad tan delta peaks indicate the formation of diffuse domains [47,48]. Both peak width [49] and peak factor are attributed to the heterogeneity or broad dispersity within the polymer [46,50]; however, peak width also correlates to the distribution of relaxation times within the polymer [51]. The parameters in Fig. 3d, obtained as depicted in Fig. 3b, highlight a correlation between the PPE content and both peak width and peak factor. This suggests the co-existence of composition-dependent acrylic-rich and PPE-rich phases within the blends.

3.2.2. Glass-fibre reinforced composite samples

Fig. 4 shows representative thermograms obtained from DMA experiments on glass fibre-reinforced PPE-modified acrylic (GF/A95/P5) matrix composite and an unmodified acrylic composite (GF/A100/P0). Prominent differences in damping behaviour are observed. The GF/A100/P0 material exhibits a distinct, single tan delta peak. In contrast, despite the observation of single peaks for the unreinforced A95/P5 in Section 3.2.1, the peak for GF/A95/P5 appears to broaden with mild evidence of peak splitting, indicating the presence of multi-species phases within the blend-matrix composite. The distance between tan delta peaks in blends correlates to the extent of phase separation between their constituents [52].

The dissimilarities in the unreinforced and reinforced A95/P5 matrix provide further evidence of the differences between the polymerisation conditions between both materials. Moreover, the effects of fibres on the growth kinetics of the polymer chains is also another possible source of variation between the two methodologies.

Although the Fox empirical model has limited applicability for blends with intermolecular interactions, it has been applied to gain preliminary insights into the plausible proportions of the hybrid matrix constituents. A similar approach has been previously reported in work by Karabanova et al. [53] who studied semi-interpenetrating polymer networks (semi-IPNs) based on polyurethane and poly(2-hydroxyethyl methacrylate), which provides insights into the structure of the polymer blends under consideration. Additionally, mass data from the solvent resistance characterisation described in Section 3.1 have been used in conjunction with the Fox equation to obtain better approximations of the compositions of the soluble and insoluble constituents of the blend. The corresponding T_g values for GF/A95/P5 are 105°C and 120°C (393 K), as shown in Fig. 4. The T_g values for neat acrylic and PPE

are 104°C (rounded value from results in Fig. 3, 377 K) and 160°C (433 K) [7], respectively. Thus, T_{g1} is most likely attributed to the presence of an acrylic homopolymer species, as evidenced by NMR spectroscopy in Fig. 7.

On the other hand, T_{g2} is a unique intermediate temperature between the two blend components, and possibly provides evidence of a reacted product of the acrylic and PPE constituents coexisting with the acrylic homopolymer. Based on the observed T_g values, the hybrid matrix system was assumed to be bi-phasic in nature, comprising an acrylic (or acrylic-rich phase) and a PPE-rich acrylic/PPE. The Fox equation was applied using Equation (1) and as detailed in Section S3.1 to estimate acrylic/PPE reacted product's composition that would give rise to a secondary glass transition temperature, T_{g2}.

$$\frac{1}{T_{gN}} = \frac{\varphi_{2,A}}{T_{gN,A}} + \frac{\varphi_{2,B}}{T_{gN,B}} \qquad (1)$$

Where $\varphi_{2,A}$ and $\varphi_{2,B}$ are mass fractions of acrylic and PPE, respectively, the sum of which equals unity; T_{gN} is the glass transition temperature corresponding to the peaks shown in Figure S8 and illustrated in Figure S9; $T_{gN,A}$ and $T_{gN,B}$ are the glass transition temperatures of the acrylic and PPE constituents, respectively. Note: all T_g values were used in Kelvin. For the determined T_{g2}, $T_{g2,A}$ and $T_{g2,B}$ values of 393 K, 377 K, and 433 K, respectively, $\varphi_{2,A}$ and $\varphi_{2,B}$ within the reacted product were estimated to be 0.69 and 0.31, respectively. The interested reader is referred to Section S3.1 for the employed procedure.

Moreover, based on the observation of two T_g values, the full blended system (S_B) can be represented by a summation of the mass fractions corresponding to T_{g1} (φ_1) and T_{g2} ($\varphi_{2,A} + \varphi_{2,B}$). T_{g1} relies solely on contributions from the acrylic phase, and T_{g2} involves contributions from both acrylic and PPE phases. Thus, assuming that all the PPE (5 wt%) within the full blended system (S_B) is directly proportional to $\varphi_{2,B}$ (0.31) according to the Fox Equation (Equation (1)), $\varphi_{2,A}$ yields a corresponding mass fraction estimate in S_B of $\left(\frac{0.69 \times 0.05}{0.31}\right) = 0.11$. The total mass fraction of acrylic/PPE reacted product is 16 wt%, based on combined acrylic and PPE mass fractions in S_B, i.e. 11 wt% and 5 wt%. Accordingly, 84% of the total 95 wt% of acrylic supplied for the polymerisation reaction was consumed in the formation of the acrylic homopolymer, whereas 16% formed a reacted product with PPE.

These results provide further evidence of the formation of a complex co-reacted acrylic/PPE species. Although no traditional cross-linker was employed as part of this study, the hybridisation of the acrylic matrix using a PPE oligomer with multiple vinyl functional groups facilitated the formation of a lightly cross-linked structure.

In light of the relative mass loss of the GF/A95/P5 sample following prolonged exposure to acetone in Section 3.1.2, these estimated mass fractions may hold the key to understanding the hybrid-matrix structure. Solvent resistance studies revealed that a mass retention of approximately 98% (of the original mass) was possible due to PPE incorporation. However, in this section, it was estimated that the acrylic homopolymer constituted 84 wt% of the full hybrid matrix system. Neat acrylic has been shown in Section 3.1.1 to be fully vulnerable to acetone attack under the same conditions. Given that solvent resistance is influenced by disengagement and reptation times of polymer chains, the blend architecture must, therefore, provide favourable shielding and trapping of entanglements, which act as anchors for a large extent of the vulnerable acrylic homopolymer [54–56].

Furthermore, changes in T_g are typically indicative of changes in chain length and mobility. The increase in T_g with the addition of PPE indicates relative reductions in chain flexibility, available free volume and chain mobility, possibly due to the contributions of
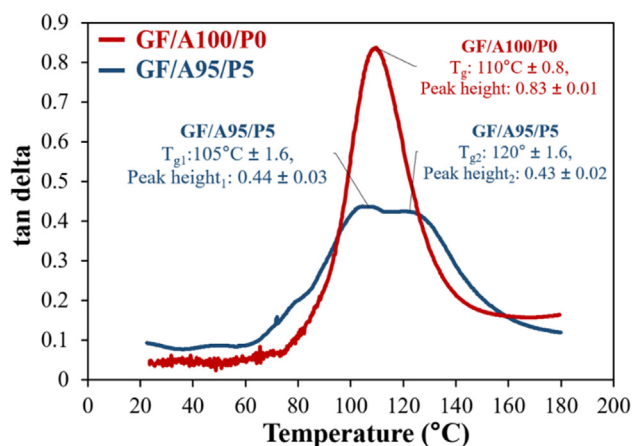

Fig. 4. Representative DMA results for glass fibre-reinforced acrylic (GF/A100/P0 – in red); and (b) PPE-modified acrylic (GF/A95/P5 – in blue) composites. Results are based on averaged duplicates (Figure S8). Lay-up: $[0]_8$. (For interpretation of the references to colour in this figure legend, the reader is referred to the web version of this article.)

phenyl moieties in the PPE and cross-links to the overall rigidity [42]. It is also apparent that the PPE-modified-matrix composite exhibited a broader peak, providing further evidence of structural and molecular heterogeneity within the matrix.

Interestingly, the severity of peak height reduction in the GF/ A95/P5 samples supports the hypothesis that the presence of cross-links and phenyl moieties within the PPE-modified acrylic composite enhances the rigidity of the matrix. Cross-links are known to give rise to reduced intensities in damping peaks [57]. Moreover, the low tan delta peak values may also provide crucial information on the fibre–matrix interfacial behaviour. It is well known that composites with poor interfacial strength exhibit superior damping ability, evidenced by increased peak heights [58,59]. Thus, a diminished peak height provides strong evidence that incorporating PPE into the acrylic matrix does not appear to deteriorate interfacial adhesion between the blend matrix and the reinforcing fibres.

3.3. Thermogravimetric analysis of unreinforced polymer and polymer blend samples

The thermal stability of the acrylic and PPE-modified acrylic blends were analysed by thermogravimetric analysis (TGA). Table 1 summarises the key results from TGA thermograms obtained for each sample. The interested reader is referred to Figure S10 for the thermograms.

Oligomeric PPE (A0/P100) appears to undergo a single-stage degradation process under the experimental conditions employed (Figure S10). Negligible mass loss was observed below 438 ± 0.1° C, its onset temperature for major degradation ($T_{onset-TGA}$). This degradation behaviour is consistent with published literature, which cite a major step between 430 and 500°C occurring due to thermal Fries-type chain rearrangements [60,61]. The incorporation of PPE delays the onset of major degradation, $T_{onset-TGA}$ by 7–10°C under the degradation conditions used. In addition to comparing the effect of PPE content on $T_{onset-TGA}$, it may be useful to compare $T_{5\%}$ and $T_{10\%}$, which are temperatures corresponding to 5% and 10% mass losses, respectively. The PPE-modified acrylic blends possessed up to 10% and 12% higher $T_{5\%}$ and $T_{10\%}$ values, respectively relative to the unmodified acrylic polymer. Thus, incorporating PPE oligomer into the acrylic polymer system results in improved thermal stability in terms of delaying thermal degradation events. However, at the PPE concentrations employed in this present work, no distinct trends or correlations were discernible between PPE loading and the extent of improvements attained. The representative DTG plots shown in Fig. 5 reveal that A100/P0 undergoes a major degradation event with a valley occurring at ca. 300–445°C. Evidence of a unique, minor degradation event in the A100/P0 material can be seen between 225°C and 300°C

Polymethylmethacrylate-based polymers are reported to undergo three-stage thermal degradation processes; with head-to-head linkage-induced scission (150°C–264°C), unsaturated chain-end-induced scission (264°C–335°C) and random main chain scission (335°C–425°C) [62–64]. However, two-stage degradations have also been previously reported [65], namely a minor event (108°C–115°C) and a major event (298°C–326°C).

In this present work, the occurrence of the unique, minor degradation event in A100/P0 between 225°C and 300°C is attributed to the degradation of unsaturated chain ends [65]. Interestingly, no preceding major degradation events were observed. The main stage of degradation occurring between 300°C and 445°C is linked to random scission of main polymer chains [62,63]. Moreover, while TGA thermograms showed minor mass losses between 90°C and 110°C for all acrylic-based polymers and blends, the early-onset degradation step reported by de Andrade Raponi et al. [65] as occurring between 150°C and 230°C was characteristically absent from the DTG thermograms of the materials in this present work. This step is induced by the breakdown of weak head-to-head linkages formed during the termination reaction (by combination) of the polymerisation process. Thus, this absence may indicate that alternative termination reactions were prevalent within the polymers under investigation [64]. The absence of this step may also suggest that shorter chain lengths dominate within each polymer material. Longer chain lengths are more susceptible to defects such as head-to-head linkages and are thus, more thermally labile [66].

Furthermore, all PPE-modified acrylic blends exhibit elevated temperature degradation events, occurring between ~ 430°C and ~ 480°C, where a slower degradation rate is evident. This late-stage event is likely due to contributions from PPE-rich phases within the blended polymer systems and may be linked with the aforementioned Fries-type rearrangements associated with PPE chains. This distinct behaviour with the blends provides strong evidence of chemical interactions between the acrylic and PPE components of the blends, mainly because thermal degradation here is driven by main chain scission. Thus, this confirms that the PPE chemically interacts with the acrylic and alters the chemical structure of the blends compared to the acrylic reference. This is further supported by the fact that the blends' end-stage degradation events coincide with the A0/P100 valley's peak temperature, as shown in Zone 1 of (Fig. 5).

3.4. Confocal Raman microscopy of fractured polymer blend surfaces

As is evident from the Confocal Raman micrographs in Fig. 6, all blends exhibit binary phase separation. PPE-rich domains appear to be dispersed within an acrylic-rich host matrix. The dispersed domains appear to vary in size, distribution and intensity within each blend. These phases appear to interact and are not mutually exclusive. Some domains exhibit a more distinct boundary,

Table 1
Summary of thermogravimetric results for acrylic polymer and PPE-modified acrylic blends showing the effects of PPE-modification on thermal stability. Values are averaged from duplicates. Parameters were obtained from data presented in Figure S10, as graphically illustrated in Figure S11.

	$T_{onset,\ TGA}$ [a] (°C)	$T_{5\%}$ [b] (°C)	$T_{10\%}$ [c] (°C)	$T_{end,\ TGA}$ [d] (°C)	M_R [e] %
A100/P0	355 ± 3.2	205 ± 6	255 ± 4.6	419 ± 1.9	1 ± 0.6
A97/P3	362 ± 1.3	216 ± 6	274 ± 4.2	426 ± 0.1	4 ± 0.0
A95/P5	362 ± 2.2	225 ± 4	282 ± 2.8	423 ± 0.9	3 ± 0.4
A90/P10	365 ± 2.8	222 ± 13	286 ± 11.2	431 ± 0.2	4 ± 0.5
A85/P15	363 ± 0.1	211 ± 2	274 ± 3.9	428 ± 1.9	4 ± 0.3
A0/P100	438 ± 0.1	426 ± 1	438 ± 0.4	471 ± 0.7	23 ± 0.1

[a,d] $T_{onset,\ TGA}$ & $T_{end,\ TGA}$: Onset & end temperatures for major degradation as determined from TGA curves, respectively (see Figure S11).
[b,c] $T_{N\%}$: Temperatures corresponding to N% mass loss using the TGA thermograms.
[e] M_R: Residual mass at the end of the thermal cycle.
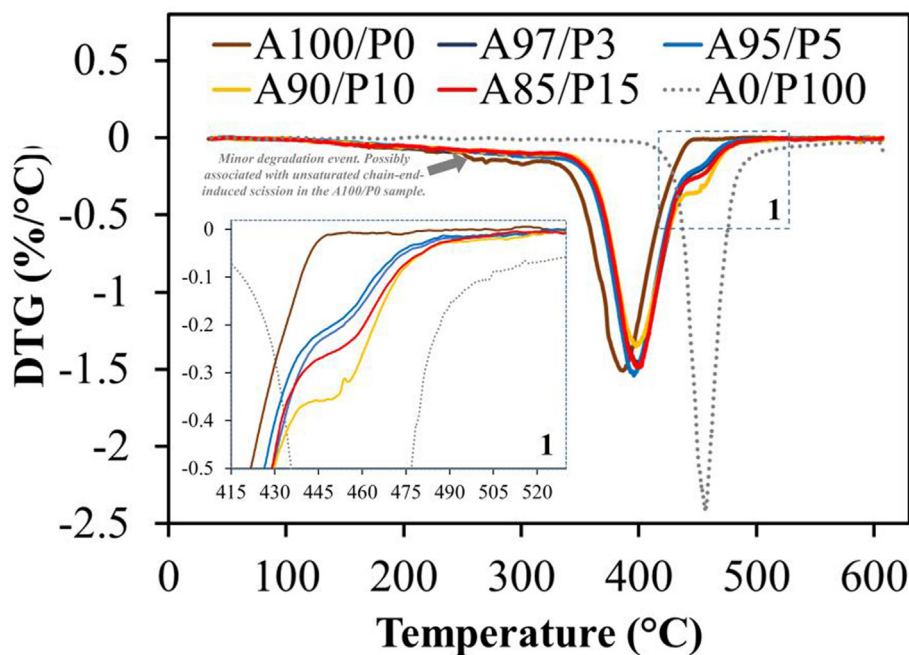
Fig. 5. Representative DTG thermograms for unmodified acrylic polymer (A100/P0), PPE oligomer (A0/P100) and their blends: A97/P3, A95/P5, A90/P10 and A85/P15. Zone 1 is an inset graph for improved visibility of unique degradation behaviour exhibited by all blends.

whereas other boundaries are more diffuse in appearance. It is worth noting that the exact proportion of each component (acrylic and PPE) within the domain and host matrix is not exactly discernible using this technique.

3.5. Solution-state nuclear magnetic resonance (NMR) spectroscopy of polymer and polymer blend samples

The chemical composition of acrylic/PPE blends A95/P5 and A90/P10 was probed by NMR spectroscopy in CDCl$_3$ and compared to monomeric and polymeric acrylic (A100/P0) and oligomeric PPE (A0/P100) in the absence and presence of BPO initiator (Fig. 7). While monomeric acrylic, polymeric acrylic and oligomeric PPE were all soluble in CDCl$_3$ at room temperature, partial dissolution of the A95/P5 and A90/P10 blends required heat (50°C), sonication (approx. 2 h) or excess CDCl$_3$. These differences in solubility suggest that A95/P5 and A90/P10 form reactive blends. Providing further evidence to support this, 95:5 and 90:10 blends (w/w) of the polymeric acrylic and oligomeric PPE were prepared by mixing the two individual components in the absence of BPO; these non-reactive blends displayed complete solubility in CDCl$_3$. These solubility differences suggest that the less soluble components of A95/P5 and A90/P10 are likely to be a high-molecular-weight copolymer or cross-linked polymeric acrylic/PPE species formed upon mixing monomeric acrylic and PPE in the presence of BPO. Both A95/P5 and A90/P10 reactive blends also exhibited noticeable swelling upon solvation in CDCl$_3$, whereas no swelling was observed with the non-reactive 95:5 and 90:10 polymeric acrylic/PPE blends (prepared in the absence of BPO). Swelling has previously been associated with the formation of cross-linked structures [41], with higher swelling ratios observed at lower cross-linker concentrations (<20%) of divinylbenzene in methyl methacrylate (MMA)-divinylbenzene cross-linked copolymers.

NMR analysis of polymeric and monomeric acrylic confirmed that polymerisation of the acrylic occurs under the reaction conditions employed to generate the reactive acrylic/PPE blends (Fig. 7). This was evidenced by the appearance of a new ^{1}H signal corresponding to –OR (R = alkyl) protons in the polymeric acrylic backbone. ^{1}H NMR analysis indicated incomplete conversion of the monomeric acrylic, which could be due to polymerisation becoming diffusion-limited upon the formation of a high-molecular-weight polymeric acrylic, the rate of radical initiator formation or the experimental conditions employed, or both (refer to supporting information for further details).

Conversely, the reaction of oligomeric PPE with BPO produced no change in the ^{1}H NMR spectrum (Fig. 7), which suggests that PPE does not homopolymerise under the reaction conditions employed. Notably, ^{1}H NMR spectra of PPE with and without BPO displayed low-intensity ^{1}H signals in the downfield region (^{1}H$^{3-5}$), which were tentatively attributed to vinylic end groups in oligomeric PPE (Fig. 7 and Figure S2).

The relative integrals of these signals suggested a 1:1 ratio of ^{1}H^3: [^{1}H^4 + ^{1}H^5], with coupling between ^{1}H^4 and ^{1}H^5 detected by COSY analysis (Figure S2). HSQC analysis indicated that the ^{1}H^3 signal correlates with a different, more downfield ^{13}C resonance compared to the ^{1}H^4 and ^{1}H^5 signals; ^{1}H^4 and ^{1}H^5 correlated with a single ^{13}C resonance within the expected ^{13}C NMR shift range for a disubstituted vinyl moiety. Therefore, the NMR analysis suggests that ^{1}H^3 protons are most likely aromatic, whereas ^{1}H^4 and ^{1}H^5 correspond to vinyl protons on disubstituted vinyl moieties in PPE oligomer end groups [67]. Using the M_n of the commercially available PPE oligomer (2300 Da), along with the relative integrals of the ^{1}H$^{3-5}$ and aromatic PPE oligomer backbone signals, suggests that the PPE oligomer contains multiple reactive aromatic vinyl end groups per chain and may, therefore, form cross-links between polymeric acrylic chains. Although these vinyl functional groups appear to be unreactive towards homopolymerisation under the conditions tested, these groups are likely involved in copolymerisation/cross-linking reactions in the presence of the acrylic monomer.

The reactivity differences between the acrylic and PPE, combined with NMR studies, suggest that the formation of block copolymers does not occur under the conditions employed in this work. The generation of random/gradient copolymers or cross-linked polymers (or both) is more likely (Fig. 8, refer to the supporting information for further details).
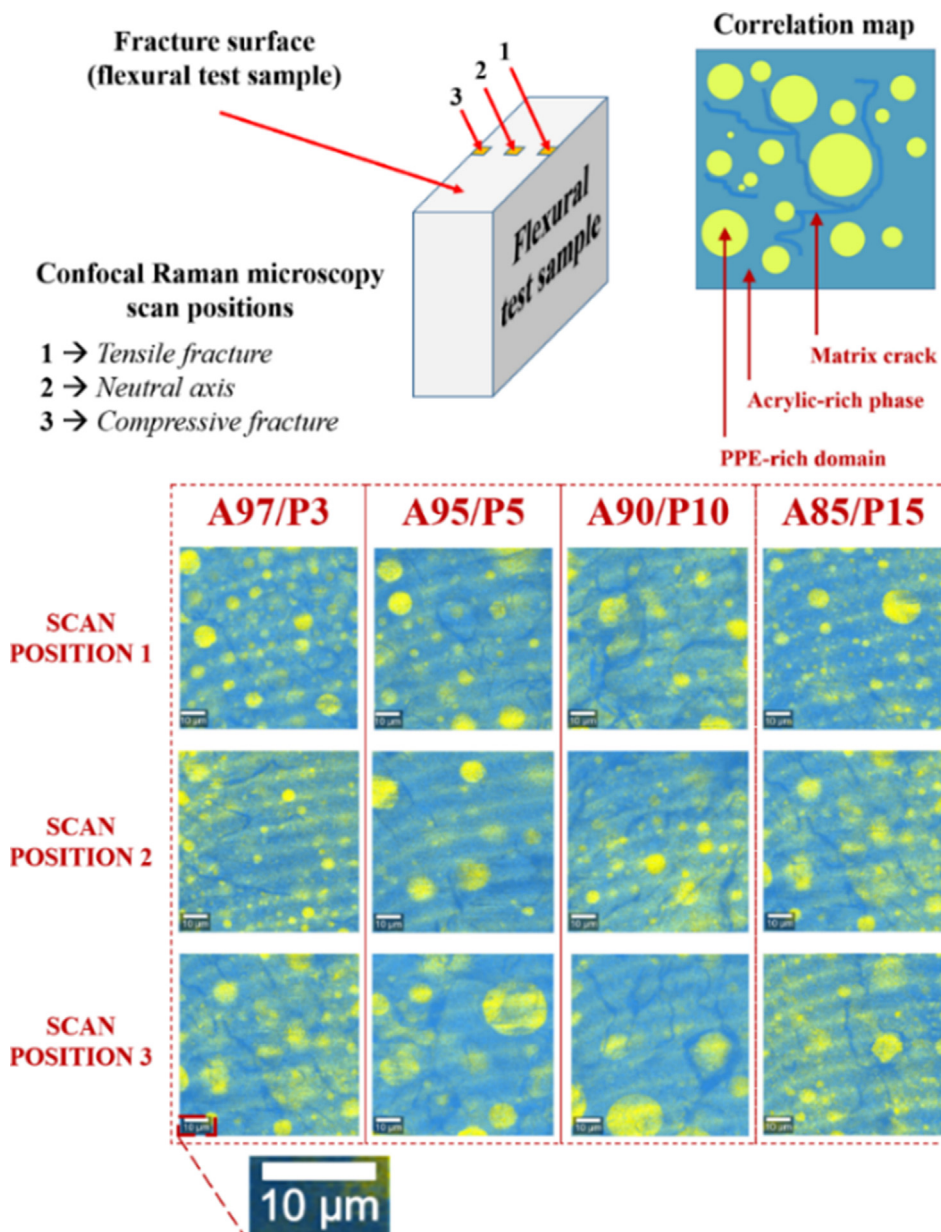
Fig. 6. Confocal Raman micrographs showing compositional maps for A97/P3, A95/P5, A90/P10 and A85/P15. Cyan and yellow regions depict an acrylic-rich phase and PPE-rich domain, respectively. (For interpretation of the references to colour in this figure legend, the reader is referred to the web version of this article.)

Although in-depth characterisation of the blends was limited by their enhanced solvent resistance in common NMR solvents, ^{1}H NMR analysis of the soluble portions of A95/P5 and A90/P10 blends indicated multi-component mixtures, which comprised polymeric acrylic, unreacted oligomeric PPE and monomeric acrylic, as well as BPO (Fig. 7, refer to supporting information for more details on the presence of BPO signals).

The same multi-component mixture was also present in the non-reactive polymer blends (95:5 and 90:10 polymeric acrylic: PPE, Figures S6 & S7, respectively). While the insoluble portions of the reactive blends (A95/P5 and A90/P10) could not be analysed, ^{1}H NMR analysis showed that the polymeric acrylic is the major component of the soluble portions (based on the relative intensities of the polymeric acrylic -OR ^{1}H NMR signal *vs*. the monomeric acrylic and oligomeric PPE). Although close inspection of baseline signals in the ^{1}H NMR spectra revealed the presence of several unknown species, these could be attributed to trace components present in the starting materials and impurities from sample

preparation (Fig. 7); none were associated with polymeric acrylic/PPE linkages. These observations were supported by DOSY NMR analysis, which revealed the presence of separate oligomeric PPE and polymeric acrylic molecules in the soluble portions of the reactive A95/P5 and A90/P10 blends, as well as the non-reactive blends, as these species give different diffusion coefficients (Figures S3 to S5).

Due to the insolubility of the reactive A95/P5 and A90/P10 blends, solid-state NMR was investigated as a method of providing further insight into the polymer structure. However, it was not possible to obtain suitably pulverised samples from the A95/P5 and A90/P10 blends using standard and cryogrinding techniques.

Taken together with the ^{1}H NMR data of the soluble components, the insolubility, resistance to mechanical grinding, and swelling of the A95/P5 and A90/P10 blends suggest that these are reactive blends, rather than (non-reactive) blended aggregates of polymeric acrylic and oligomeric PPE. Indeed, the enhanced solvent resistance and swelling suggest the formation of high-
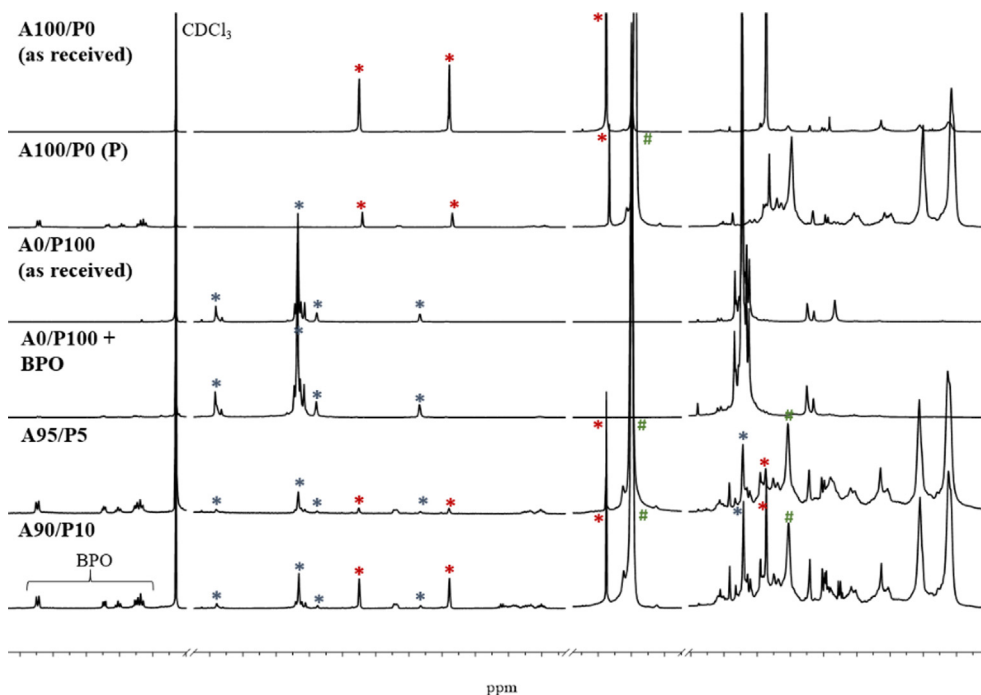
Fig. 7. Overlaid ^{1}H NMR spectra of the acrylic/PPE blends A95/P5 and A90/P10 and the starting materials in the presence and absence of BPO in CDCl$_3$. The key ^{1}H NMR signals from the monomeric acrylic (*, red), oligomeric PPE (*, blue) and polymeric acrylic (#, green) are highlighted. (For interpretation of the references to colour in this figure legend, the reader is referred to the web version of this article.)

molecular-weight copolymeric or cross-linked acrylic/PPE species. While the resistance to mechanical grinding and lack of solubility limited determination of the precise chemical structure of the A95/P5 and A90/10 blends by both solid- and solution-state NMR spectroscopy, this low solubility implies potential benefits in terms of solvent resistance. Moreover, the observed resistance to pulverisation in the blends suggests enhanced mechanical properties.

3.6. Proposed polymer blend architecture

Based on a vinyl functionality of 1.9 for the PPE formulation (specified by the manufacturer [68]), the formation of cross-linked acrylic/PPE species is highly likely within the blends based on the number of reactive sites as shown in Fig. 9.
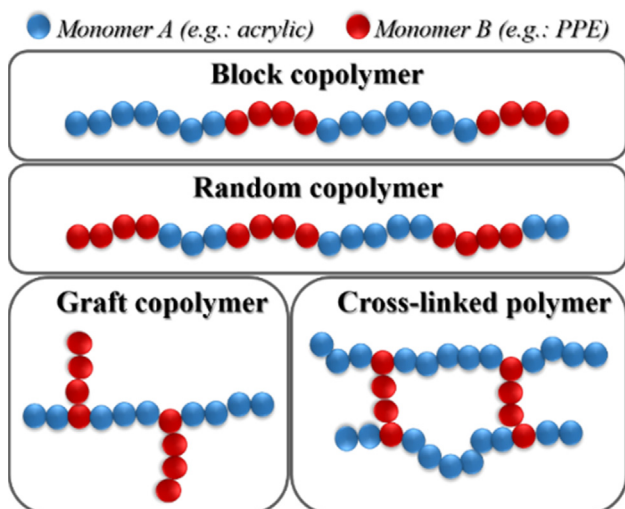

Fig. 8. General structures of block, random and graft copolymers and cross-linked polymers.

Moreover, as discussed in Section 3.5, the PPE grade used cannot homopolymerise; meaning no PPE-PPE interactions are expected during the polymerisation process. Instead, the telechelicity of PPE facilitates its participation in the propagation reaction with growing acrylic chains.

The study illustrated in Fig. 10a was conducted to explore the effects of the presence of crosslinks on the reshapability of the blends. As shown in Fig. 10b, these trials revealed that the presence of cross-links did not have deleterious effects on the post-
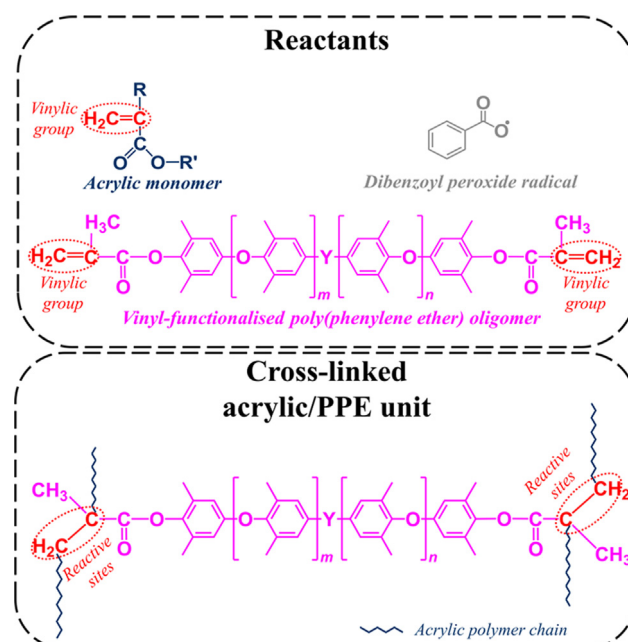
Fig. 9. Chemical structures of the reactants (acrylic monomer, PPE oligomer and dibenzoyl peroxide radical) and the proposed cross-linked acrylic/PPE structure formed.
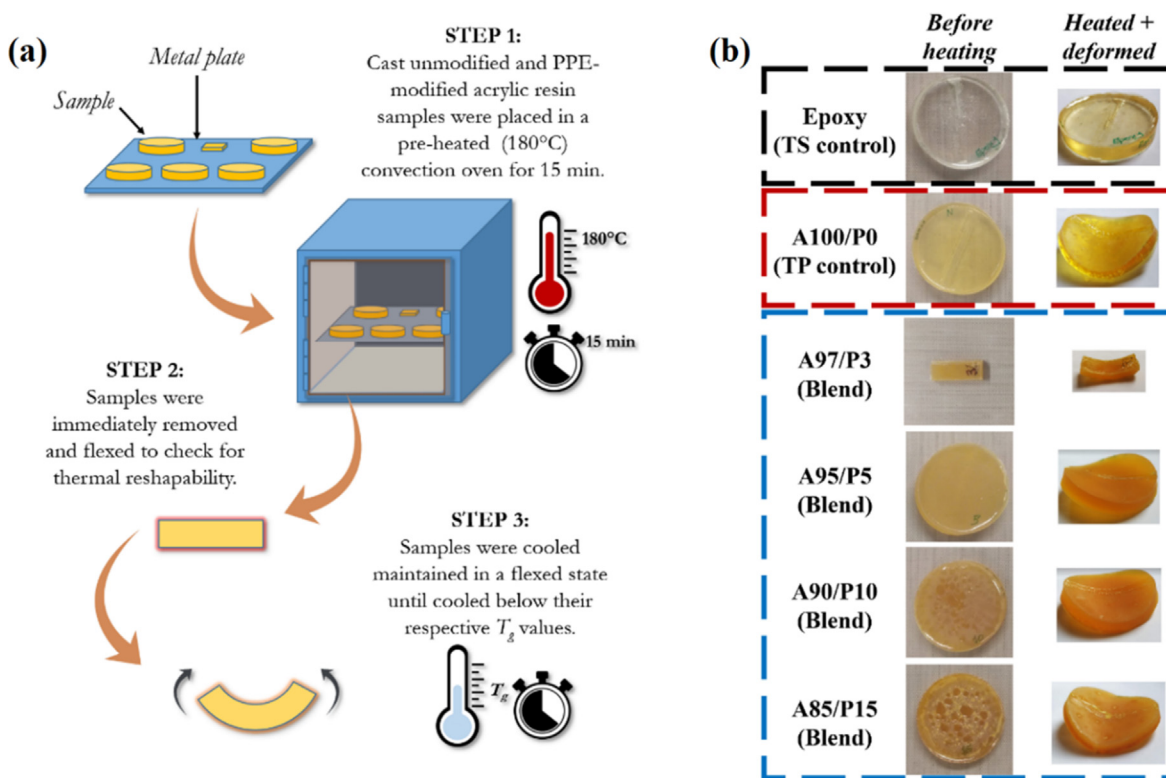
Fig. 10. (a) Methodology and (b) results of reshapability trials performed on unreinforced neat and PPE-modified acrylic samples. 40-mm dia. disc samples were used for an epoxy reference, A100/P0, A95/P5, A90/P10 and A85/P15 samples. The sample for A97/P3 measures 25 mm × 8 mm × 4 mm due to material availability constraints.

processibility of the unreinforced PPE-modified acrylic blends. The unreinforced acrylic/PPE blends and the unreinforced neat acrylic samples can be seen to be deformable upon heating and retain the deformed shape upon cooling. Thus, it was demonstrated that the thermoplastic blends produced in this work exhibit the desirable characteristics of thermosets (possessing excellent solvent resistance, thermal stability, and easy infusibility at room temperature), while also retaining the post-processibility of thermoplastics.

Such duality of characteristics has been previously reported for materials such as vitrimers and covalent adaptable networks (CANs), which are known to offer excellent reprocessibility despite containing cross-linked networks [69–71]. In addition to retaining the post-processibility of thermoplastics, which facilitates reshaping even after polymerisation and solidification, these attributes are highly advantageous and offer numerous potentials for composite applications.

Combined with the micrographic evidence from confocal Raman imaging and SEM imaging, thermogravimetric analysis and solvent resistance trials, the thermoformability of these blends confirms that both acrylic-rich and cross-linked acrylic/PPE remain reshapable following in-situ polymerisation and consolidation. Moreover, the results of thermoforming trials suggest a good extent of chain mobility must be possible despite the presence of cross-links. Thus, these results confirm that the blends may only be slightly cross-linked or that the cross-links form clusters.

The degree and density of cross-linking are expected to be highly influenced by the relative reactivities of PPE and acrylic. Variations in the extent of steric hindrance resulting from the presence of bulky phenyl groups [72,73] will likely result in volumetric congestion around each successive acrylic/PPE interaction at the reactive site. In addition, an increase in the solution viscosity is expected to result in the trapping or burying of some substituents. Consequently, some of the PPE macromolecules may only be par-

tially saturated upon the termination of the polymerisation reaction, with perhaps trace amounts of unreacted PPE remaining entrapped by cross-linked and grafted chains. The latter may account for the aforementioned observation of unreacted PPE during NMR analysis. Branched or grafted chains can effectively become anchored and trapped within the network within such structures, restricting disengagement. As such, their presence is not expected to compromise the solvent resistance of the blends [74].

Moreover, no specialised approach was adopted for tuning or controlling the cross-linking or grafting processes; thus, spatial variations are expected within each blend system. Finally, based on these observations and discussions, the chain architecture is proposed in Fig. 11.

This is supported by the analysis of results presented in Section 3.1.2, where the two distinct glass transition temperatures observable at the tan delta peaks provided evidence of the formation of a complex reacted acrylic/PPE species. Although these temperatures revealed that the acrylic homopolymer contributed approximately 84 wt% of the total blended system within the GF/A95/P5 material, with the reacted product constituting approximately 16 wt%, the relatively high residual mass following exposure to acetone provides even more insights into the blend architecture. The linear, acrylic homopolymer is likely shielded within a protective reacted network and is expected to interpenetrate the cross-linked acrylic/PPE network alongside a graft copolymer. In such a structure, the network can effectively serve as a scaffold and may promote a great extent of entanglement between linear acrylic and PPE-grafted acrylic chains.

Remarkably, such architecture has been previously reported by Röttger [75], who showed that dioxaborolane-based vitrimers exhibit excellent solvent resistance in THF, retaining up to 95% of their original mass. The same materials were reported to remain thermoformable even with cross-linked constituents. This is simi-
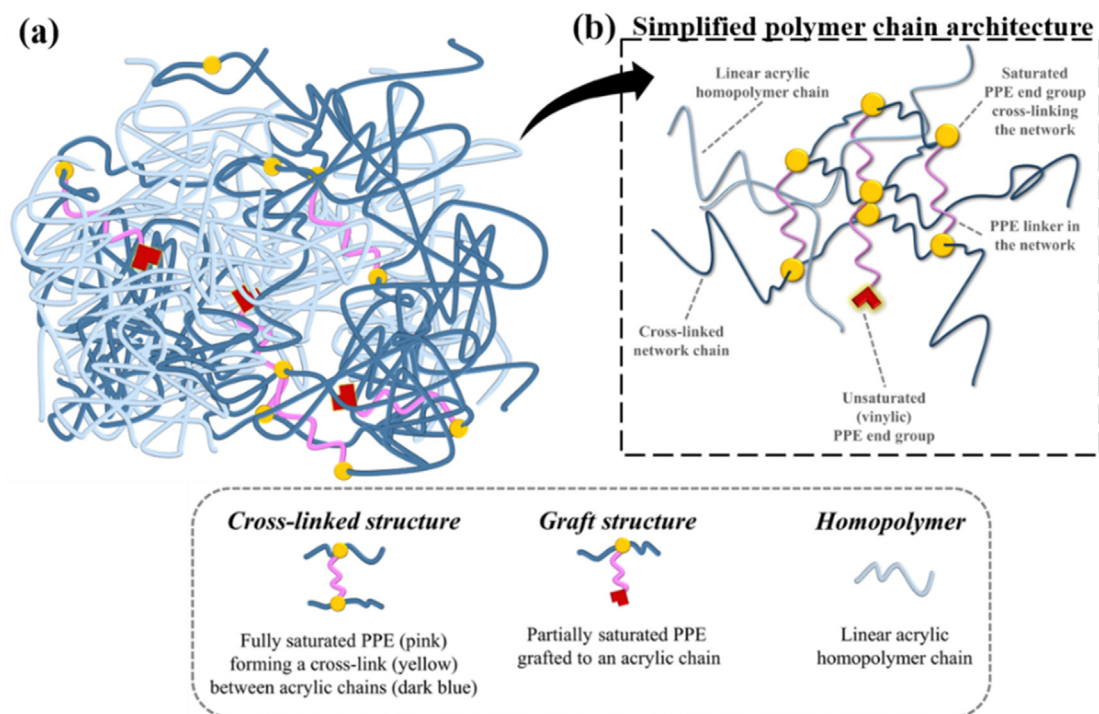
Fig. 11. (a) The proposed polymer architecture within the PPE-modified acrylic blends, showing a lightly cross-linked acrylic/PPE network, a branched or grafted acrylic/PPE species, and a highly entangled, linear acrylic polymer species; (b) a simplified form of same.

lar to the findings presented herein and may provide interesting insights into the behaviour of the blends considered in this present work. The formation of a vitrimer is highly unexpected, however, as vitrimers characteristically require ester-alcohol transesterification reactions. Thus, it is not believed that the blends in this work are vitrimeric in nature.

Moreover, the process employed in this paper produces a similar material to interpenetrating polymer networks (IPNs) in that at least one of the polymers is synthesised in the presence of the other [53,76–80]. A distinguishing characteristic of IPNs is that one (semi-IPN) or both (full IPN) are cross-linked to form a network. Although the novel polymer blends presented in this chapter were not prepared with a traditional cross-linker, it has been shown that the telechelic PPE employed can promote cross-linking. Thus, the resulting blend architecture is likely similar to a semi-IPN with both linear acrylic and branched/grafted acrylic/PPE species interpenetrating within a lightly cross-linked acrylic/PPE network.

4. Conclusions

This paper demonstrates a simple, yet practical reactive hybridisation approach for tailoring the performance of liquid acrylic resins for composite applications. Unique insights into the structure–property relationships, which underpin the observed effects of hybridisation, were provided via a combination of spectroscopic, thermal and microscopic analytical techniques. Incorporating reactive oligomeric PPE with functional vinylic groups into reactive monomeric acrylic resin results in enhanced solvent resistance (in $CDCl_3$ and acetone) and higher glass transition temperature of unreinforced (up to 6% increase) and glass fibre-reinforced (+9%) acrylic/PPE hybrid material systems, with respect to their neat acrylic counterparts. While unreinforced blend samples retained up to 77% of their original masses after 72 h of acetone exposure, the unreinforced, unmodified acrylic sample fully dissolved after 300 min. Reinforced samples exhibited similar trends: 98% and 72% mass-retentions in the PPE-modified and unmodified

samples, respectively. In addition to the enhanced solvent resistance, the hybrids exhibited exceptional resistance to mechanical grinding; thus, suitable samples for solid-state NMR spectroscopic analysis were not readily obtained. However, solution-state NMR spectroscopic analysis of the soluble portions (in $CDCl_3$) indicated the formation of multi-component mixtures comprising individual molecules of monomeric and polymeric acrylic, oligomeric PPE and BPO. This suggests that the insoluble portions are more complex and likely to be copolymeric or cross-linked acrylic/PPE species while retaining reshapability with applied heat and pressure after in-situ polymerisation. These findings open up new opportunities for scalable and low-temperature fabrication of thermoplastic amorphous hybrid-matrix composites with tailored properties for a wide range of practical applications. Finally, while this work demonstrated positive hybridisation effects using only glass fibres, we believe that the insights presented herein should be applicable to other appropriately sized fibre systems (for the base reactive acrylic resin).

Declaration of Competing Interest

The authors declare that they have no known competing financial interests or personal relationships that could have appeared to influence the work reported in this paper.

Acknowledgements

Data availability

The raw data required to reproduce these findings cannot be shared at this time due to technical or time limitations.

Appendix A. Supplementary material

Supplementary data to this article can be found online at https://doi.org/10.1016/j.matdes.2021.109804.

References

[1] W. Obande, C.M. Ó Brádaigh, D. Ray. Continuous fibre-reinforced thermoplastic acrylic-matrix composites prepared by liquid resin infusion – A review. Compos Part B Eng 2021:108771. https://doi.org/10.1016/j.compositesb.2021.108771

[2] N. Han, I. Baran, J.S.M. Zanjani, O. Yuksel, L.L. An, R. Akkerman, Experimental and computational analysis of the polymerization overheating in thick glass/Elium® acrylic thermoplastic resin composites, Compos Part B Eng (2020), https://doi.org/10.1016/j.compositesb.2020.108430.

[3] S.K. Bhudolia, G. Gohel, L.K. Fai, R.J. Barsotti, Investigation on ultrasonic welding attributes of novel carbon/Elium® composites, Materials (Basel) 13 (2020) 10–15, https://doi.org/10.3390/ma13051117.

[4] S.K. Bhudolia, G. Gohel, L. Kah Fai, R.J. Barsotti, Fatigue response of ultrasonically welded carbon/Elium® thermoplastic composites, Mater Lett 264 (2020), https://doi.org/10.1016/j.matlet.2020.127362 127362.

[5] M.E. Kazemi, L. Shanmugam, S. Chen, L. Yang, J. Yang, Novel thermoplastic fiber metal laminates manufactured with an innovative acrylic resin at room temperature, Compos Part A Appl Sci Manuf 138 (2020) 106043, https://doi.org/10.1016/j.compositesa.2020.106043.

[6] M.E. Kazemi, L. Shanmugam, Z. Li, R. Ma, L. Yang, J. Yang, Low-velocity impact behaviors of a fully thermoplastic composite laminate fabricated with an innovative acrylic resin, Compos Struct 250 (2020) 112604, https://doi.org/10.1016/j.compstruct.2020.112604.

[7] H. Bel Haj Frej, R. Léger, D. Perrin, P. Ienny, Effect of aging temperature on a thermoset-like novel acrylic thermoplastic composite for marine vessels, J Compos Mater (2021), https://doi.org/10.1177/0021998321996780. 002199832199678.

[8] L. Shanmugam, M.E. Kazemi, C. Qiu, M. Rui, L. Yang, J. Yang, Influence of UHMWPE fiber and Ti6Al4V metal surface treatments on the low-velocity impact behavior of thermoplastic fiber metal laminates, Adv Compos Hybrid Mater 3 (2020) 508–521, https://doi.org/10.1007/s42114-020-00189-7.

[9] S.K. Bhudolia, G. Gohel, S.C. Joshi, K.F. Leong, Quasi-static indentation response of core-shell particle reinforced novel NCCF/Elium® composites at different feed rates, Compos Commun 21 (2020) 100383, https://doi.org/10.1016/j.coco.2020.100383.

[10] A. Chilali, W. Zouari, M. Assarar, H. Kebir, R. Ayad, Analysis of the mechanical behaviour of flax and glass fabrics-reinforced thermoplastic and thermoset resins, J Reinf Plast Compos 35 (2016) 1217–1232, https://doi.org/10.1177/0731684416645203.

[11] G. Kinvi-Dossou, R. Matadi Boumbimba, N. Bonfoh, S. Garzon-Hernandez, D. Garcia-Gonzalez, P. Gerard, et al., Innovative acrylic thermoplastic composites versus conventional composites: Improving the impact performances, Compos Struct 217 (2019) 1–13, https://doi.org/10.1016/j.compstruct.2019.02.090.

[12] A. Aronica, D. Fossati, Mechanical Properties of Carbon Fiber Composite Materials, Politecnico di Milano [Master's Thesis] (2014).

[13] A. Aronica, D. Fossati, Effects of resin and processing on mechanical properties of carbon fibre composites, Politecnico di Milano [Master's Thesis] (2015).

[14] C. Baley, M. Lan, A. Bourmaud, A. Le Duigou, Compressive and tensile behaviour of unidirectional composites reinforced by natural fibres: Influence of fibres (flax and jute), matrix and fibre volume fraction, Mater Today Commun 16 (2018) 300–306, https://doi.org/10.1016/j.mtcomm.2018.07.003.

[15] W. Obande, D. Ray, C.M. Ó Brádaigh. Viscoelastic and drop-weight impact properties of an acrylic-matrix composite and a conventional thermoset composite – A comparative study. Mater Lett 2019;238:38–41. https://doi.org/10.1016/j.matlet.2018.11.137

[16] A. Chilali, M. Assarar, W. Zouari, H. Kebir, R. Ayad, Effect of geometric dimensions and fibre orientation on 3D moisture diffusion in flax fibre reinforced thermoplastic and thermosetting composites, Compos Part A Appl Sci Manuf 95 (2017) 75–86, https://doi.org/10.1016/j.compositesa.2016.12.020.

[17] S.K.K. Bhudolia, P. Perrotey, S.C.C. Joshi, Optimizing polymer infusion process for thin ply textile composites with novel matrix system, Materials (Basel) 10 (2017), https://doi.org/10.3390/ma10030293.

[18] T. Lorriot, J. El Yagoubi, J. Fourel, F. Tison. Non-conventional glass fiber NCF composites with thermoset and thermoplastic matrices. 20th Int. Conf. Compos. Mater., Copenhagen: 2015

[19] W. Obande, D. Mamalis, D. Ray, L. Yang, C.M. Ó Brádaigh. Mechanical and thermomechanical characterisation of vacuum-infused thermoplastic- and thermoset-based composites. Mater Des 2019;175:107828. https://doi.org/10.1016/j.matdes.2019.107828

[20] R.E. Murray, D. Penumadu, D. Cousins, R. Beach, D. Snowberg, D. Berry, et al., Manufacturing and Flexural Characterization of Infusion-Reacted Thermoplastic Wind Turbine Blade Subcomponents, Appl Compos Mater 27 (2019) 1–17, https://doi.org/10.1007/s10443-019-9760-2.

[21] P. Davies, M. Arhant, Fatigue behaviour of acrylic matrix composites: influence of seawater, Appl Compos Mater 26 (2019) 507–518, https://doi.org/10.1007/s10443-018-9713-1.

[22] S.K. Bhudolia, P. Perrotey, S.C. Joshi, Mode I fracture toughness and fractographic investigation of carbon fibre composites with liquid Methylmethacrylate thermoplastic matrix, Compos Part B Eng 134 (2018) 246–253, https://doi.org/10.1016/j.compositesb.2017.09.057.

[23] Chemical Resistance of Thermoplastics, Plastics Design Library, Volume 1, 2012, p. 1–106. https://doi.org/10.1016/b978-1-4557-7896-6.00001-7.

[24] P.K. Mallick, Thermoplastics and thermoplastic-matrix composites for lightweight automotive structures, Mater. Des. Manuf. Light. Veh., Elsevier Ltd. (2010) 174–207, https://doi.org/10.1533/9781845697822.1.174.

[25] S.E. Lee, E. Jeong, M.Y. Lee, M.K. Lee, Y.S. Lee, Improvement of the mechanical and thermal properties of polyethersulfone-modified epoxy composites, J Ind Eng Chem 33 (2016) 73–79, https://doi.org/10.1016/j.jiec.2015.09.022.

[26] K. Mimura, H. Ito, H. Fujioka, Improvement of thermal and mechanical properties by control of morphologies in PES-modified epoxy resins, Polymer (Guildf) 41 (2000) 4451–4459, https://doi.org/10.1016/S0032-3861(99)00700-4.

[27] P. Zhao, X. Liang, J. Chen, Q. Ran, Y. Gu, Poly(ether imide)-modified benzoxazine blends: Influences of phase separation and hydrogen bonding interactions on the curing reaction, J Appl Polym Sci 128 (2013) 2865–2874, https://doi.org/10.1002/app.38459.

[28] N. Biolley, T. Pascal, B. Sillion, Polyimide-modified epoxy system: time-temperature-transformation diagrams, mechanical and thermal properties, Polymer (Guildf) 35 (1994) 558–564, https://doi.org/10.1016/0032-3861(94)90511-8.

[29] I. Hamerton, L.T. McNamara, B.J. Howlin, P.A. Smith, P. Cross, S. Ward, Toughening mechanisms in aromatic polybenzoxazines using thermoplastic oligomers and telechelics, Macromolecules 47 (2014) 1946–1958, https://doi.org/10.1021/ma5002436.

[30] T. Orhan, S. Ates, J. Hacaloglu, Y. Yagci, Thermal degradation characteristics of polysulfones with benzoxazine end groups, J Anal Appl Pyrolysis 94 (2012) 146–152, https://doi.org/10.1016/j.jaap.2011.12.001.

[31] B. Del Saz-Orozco, D. Ray, A. Kervennic, P.T. McGrail, W.F. Stanley, Toughening of carbon fibre/polybenzoxazine composites by incorporating polyethersulfone into the interlaminar region, Mater Des 93 (2016) 297–303, https://doi.org/10.1016/j.matdes.2015.12.138.

[32] G. Di Pasquale, O. Motta, A. Recca, J.T. Carter, P.T. McGrail, D. Acierno, New high-performance thermoplastic toughened epoxy thermosets, Polymer (Guildf) 38 (1997) 4345–4348, https://doi.org/10.1016/S0032-3861(96)01031-2.

[33] I. Hamerton, L.T. McNamara, B.J. Howlin, P.A. Smith, P. Cross, S. Ward, Developing toughened aromatic polybenzoxazines using thermoplastic oligomers and telechelics, part 1: Preparation and characterization of the functionalized oligomers, J Appl Polym Sci (2014;131.), https://doi.org/10.1002/app.40875.

[34] B. Ronak. Fracture mechanics of nanostructured polymer blends with janus particles. University of Bayreuth [Doctoral Thesis], 2018.

[35] Nelissen LNIH. A novel route to blends of polystyrene and poly(2,6-dimethyl-1,4-phenylene ether) : synthesis, properties and applications 1991. https://doi.org/10.6100/IR352941.

[36] J.G. Bennett, R.M. Summers, Composition of a polyphenylene ether and an acrylic resin modified polyisoprene (1974), https://doi.org/10.1145/178951.178972.

[37] F.J. Viersen, P. Colantuoni, I. Mamalis, Compatibilization of poly(2,6-dimethyl-1,4-phenylene ether)/poly(vinylidene difluoride) blends, Die Angew Makromol Chemie (1993), https://doi.org/10.1002/apmc.1993.052060111.

[38] W. Obande, C.M. Ó Brádaigh , D. Ray. Thermoplastic hybrid-matrix composite prepared by a room-temperature vacuum infusion and in-situ polymerisation process. Compos Commun 2020. https://doi.org/10.1016/j.coco.2020.100439

[39] I. Devotta, M.V. Badiger, P.R. Rajamohanan, S. Ganapathy, R.A. Mashelkar, Unusual retardation and enhancement in polymer dissolution: role of disengagement dynamics, Chem Eng Sci 50 (1995) 2557–2569.

[40] B.A. Miller-Chou, J.L. Koenig, A review of polymer dissolution, Prog Polym Sci 28 (2003) 1223–1270, https://doi.org/10.1016/S0079-6700(03)00045-5.

[41] F.M. Uhl, G.F. Levchik, S.V. Levchik, C. Dick, J.J. Liggat, C.E. Snape, et al., Thermal stability of cross-linked polymers: Methyl methacrylate with divinylbenzene and styrene with dimethacrylates, Polym Degrad Stab 71 (2001) 317–325, https://doi.org/10.1016/S0141-3910(00)00181-6.

[42] T. Nakano, π-stacked polymers and molecules: Theory, synthesis, and properties. (2014), https://doi.org/10.1007/978-4-431-54129-5.

[43] M. Zhang, O. Bareille, M. Salvia, Cure and damage monitoring of flax fiber-reinforced epoxy composite repairs for civil engineering structures using embedded piezo micro-patches, Constr Build Mater (2019), https://doi.org/10.1016/j.conbuildmat.2019.07.179.

[44] C.C. Huang, M.S. Yang, M. Liang, Synthesis of new thermosetting poly(2,6-dimethyl-1, 4-phenylene oxide)s containing epoxide pendant groups, J Polym Sci Part A Polym Chem (2006), https://doi.org/10.1002/pola.21679.

[45] J.P. Correa-Aguirre, F. Luna-Vera, C. Caicedo, B. Vera-Mondragón, M.A. Hidalgo-Salazar, The Effects of Reprocessing and Fiber Treatments on the Properties of Polypropylene-Sugarcane Bagasse Biocomposites, Polymers (Basel) 12 (2020) 1440, https://doi.org/10.3390/polym12071440.

[46] A. Romo-Uribe, Dynamic Mechanical Thermal Analysis of Epoxy/Thermoplastic Blends 23, Handb. Epoxy Blends (2017) 675–706, https://doi.org/10.1007/978-3-319-40043-3_23.

[47] K.S. Arora, F. Baah, G.M. Canard, D.E. Setze, DMA of new acrylic- polyurethane hybrids, Eur Coatings J (2001). 2001.

[48] N.J.W. Gamage, D.J.T. Hill, C.A. Lukey, P.J. Pomery, Thermal characterization of polyester-melamine coating matrices prepared under nonisothermal conditions, J Polym Sci Part A Polym Chem 41 (2003) 1603–1621, https://doi.org/10.1002/pola.10698.

[49] A. Bacchi, J.A. Yih, J. Platta, J. Knight, C.S. Pfeifer, Shrinkage/stress reduction and mechanical properties improvement in restorative composites formulated with thio-urethane oligomers, J Mech Behav Biomed Mater 78 (2018) 235–240, https://doi.org/10.1016/j.jmbbm.2017.11.011.

[50] H. Miyagawa, M.J. Rich, L.T. Drzal, Amine-cured epoxy/clay nanocomposites. I. Processing and chemical characterization, J Polym Sci Part B Polym Phys (2004), https://doi.org/10.1002/polb.20288.

[51] A.R. Kannurpatti, J.W. Anseth, C.N. Bowman, A study of the evolution of mechanical properties and structural heterogeneity of polymer networks formed by photopolymerizations of multifunctional (meth)acrylates, Polymer (Guildf) 39 (1998) 2507–2513, https://doi.org/10.1016/S0032-3861(97)00585-5.

[52] N. Alizadeh, M. Barde, M. Minkler, A.D. Celestine, V. Agrawal, B. Beckingham, et al., High-fracture-toughness acrylic–polyurethane-based graft-interpenetrating polymer networks for transparent applications, Polym Int (2020), https://doi.org/10.1002/pi.6149.

[53] L.V. Karabanova, G. Boiteux, G. Seytre, S. Isabelle, A.W. Lloyd, S.V. Mikhalovsky, et al., Phase separation in the polyurethane/poly(2-hydroxyethyl methacrylate) semi-interpenetrating polymer networks synthesized by different ways, Polym Eng Sci 48 (2008) 588–597, https://doi.org/10.1002/pen.

[54] T. Fujiyabu, Y. Yoshikawa, Chung U il, T. Sakai. Structure-property relationship of a model network containing solvent. Sci Technol Adv Mater 2019. https://doi.org/10.1080/14686996.2019.1618685.

[55] L.G.D. Hawke, M. Ahmadi, H. Goldansaz, E. van Ruymbeke, Viscoelastic properties of linear associating poly(n-butyl acrylate) chains, J Rheol (N Y N Y) (2016), https://doi.org/10.1122/1.4942231.

[56] C. Huang, G. Huang, S. Li, M. Luo, H. Liu, X. Fu, et al., Research on architecture and composition of natural network in natural rubber, Polymer (Guildf) (2018), https://doi.org/10.1016/j.polymer.2018.08.057.

[57] K. Bandzierz, L. Reuvekamp, J. Dryzek, W. Dierkes, A. Blume, D. Bielinski, Influence of network structure on glass transition temperature of elastomers, Materials (Basel) (2016;9.), https://doi.org/10.3390/MA9070607.

[58] D. Romanzini, A. Lavoratti, H.L. Ornaghi, S.C. Amico, A.J. Zattera, Influence of fiber content on the mechanical and dynamic mechanical properties of glass/ramie polymer composites, Mater Des 47 (2013) 9–15, https://doi.org/10.1016/j.matdes.2012.12.029.

[59] M. Idicula, S.K. Malhotra, K. Joseph, S. Thomas, Dynamic mechanical analysis of randomly oriented intimately mixed short banana/sisal hybrid fibre reinforced polyester composites, Compos Sci Technol 65 (2005) 1077–1087, https://doi.org/10.1016/j.compscitech.2004.10.023.

[60] E.N. Peters, Poly(phenylene ether) based amphiphilic block copolymers, Polymers (Basel) 9 (2017), https://doi.org/10.3390/polym9090433.

[61] G. Wypych, Data on Specific Polymers, Handb Mater Weather (2013) 351–546, https://doi.org/10.1016/b978-1-895198-62-1.50017-2.

[62] S.G. Castellanos, V.V.A. Fernández, J. Aguilar, F.J. Moscoso-Sánchez, I. Ceja, G. Canché-Escamilla, et al., Synthesis and characterization of poly(methyl methacrylate)-boehmite nanocomposites by direct microemulsion polymerization combined with the in-situ sol-gel method, Polymer (Guildf) 163 (2019) 134–143, https://doi.org/10.1016/j.polymer.2018.12.053.

[63] E.T. Röchow, L. Häußler, A. Korwitz, D. Pospiech, Thermal decomposition of phosphonate-containing methacrylate-based copolymers, Polym Degrad Stab 152 (2018) 235–243, https://doi.org/10.1016/j.polymdegradstab.2018.04.036.

[64] W. Viratyaporn, R.L. Lehman, Effect of nanoparticles on the thermal stability of PMMA nanocomposites prepared by in situ bulk polymerization, J Therm Anal Calorim 103 (2011) 267–273, https://doi.org/10.1007/s10973-010-1051-y.

[65] Raponi O de Andrade, L.C.M. Barbosa, B.R. de Souza, A.C. Ancelotti Junior, Study of the influence of initiator content in the polymerization reaction of a thermoplastic liquid resin for advanced composite manufacturing, Adv Polym Technol 37 (2018) 3579–3587, https://doi.org/10.1002/adv.22142.

[66] V. Percec, C. Pugh, O. Nuyken, Pask SD. Macromonomers, Oligomers and Telechelic Polymers, Compr. Polym. Sci. Suppl., Elsevier (1989) 281–357, https://doi.org/10.1016/b978-0-08-096701-1.00189-0.

[67] H.J. Reich, Chem 605 - Structure Determination Using Spectroscopic, Methods (2020).

[68] SABIC. NORYLTM SA9000 resin solubility guide 2019.

[69] H. Han, X. Xu, Poly(methyl methacrylate)–epoxy vitrimer composites, J Appl Polym Sci (2018), https://doi.org/10.1002/app.46307.

[70] Q. Li, S. Ma, N. Lu, J. Qiu, J. Ye, Y. Liu, et al., Concurrent thiol–ene competitive reactions provide reprocessable, degradable and creep-resistant dynamic–permanent hybrid covalent networks, Green Chem (2020), https://doi.org/10.1039/d0gc02823a.

[71] N.J. Van Zee, R. Nicolaÿ, Vitrimers: Permanently crosslinked polymers with dynamic network topology, Prog Polym Sci (2020), https://doi.org/10.1016/j.progpolymsci.2020.101233.

[72] Flory PJ. Principles of polymer chemistry. 1953.

[73] B. Yamada, P.B. Zetterlund, E. Sato, Utility of propenyl groups in free radical polymerization: Effects of steric hindrance on formation and reaction behavior as versatile intermediates, Prog Polym Sci 31 (2006) 835–877, https://doi.org/10.1016/j.progpolymsci.2006.08.005.

[74] R.A. Plenderleith, C.J. Pateman, C. Rodenburg, J.W. Haycock, F. Claeyssens, C. Sammon, et al., Arginine-glycine-aspartic acid functional branched semi-interpenetrating hydrogels, Soft Matter (2015), https://doi.org/10.1039/c5sm00695c.

[75] M. Röttger, T. Domenech, R. Van Der Weegen, A. Breuillac, R. Nicolaÿ, L. Leibler, High-performance vitrimers from commodity thermoplastics through dioxaborolane metathesis, Science 356 (2017) 62–65, https://doi.org/10.1126/science.aah5281.

[76] V.D. Athawale, S.L. Kolekar, S.S. Raut, Recent developments in polyurethanes and poly(acrylates) interpenetrating polymer networks, J Macromol Sci - Polym Rev (2003), https://doi.org/10.1081/MC-120018018.

[77] L.V. Karabanova, S.V. Mikhalovsky, A.W. Lloyd, G. Boiteux, L.M. Sergeeva, T.I. Novikova, et al., Gradient semi-interpenetrating polymer networks based on polyurethane and poly(vinyl pyrrolidone), J Mater Chem (2005), https://doi.org/10.1039/b410178b.

[78] L.H. Sperling, V. Mishra, The current status of interpenetrating polymer networks, Polym Adv Technol (1996), https://doi.org/10.1002/(SICI)1099-1581(199604)7:4<197::AID-PAT514>3.0.CO;2-4.

[79] L.H. Sperling, R. Hu, Interpenetrating polymer networks. Polym. Blends Handb. (2014), https://doi.org/10.1007/978-94-007-6064-6_8.

[80] Y.S. Lipatov, T.S. Chramova, L.M. Sergeeva, L.V. Karabanova, Some properties of intermediate regions in interpenetrating polymeric networks, J. Polym. Sci. Polym. Chem. Ed (1977), https://doi.org/10.1002/pol.1977.170150216.